PERGAMON

International Journal of Solids and Structures 39 (2002) 3039–3055

INTERNATIONAL JOURNAL OF SOLIDS and STRUCTURES

www.elsevier.com/locate/ijsolstr

Buckling behavior of stiffened laminated plates

Mei-Wen Guo [a], Issam E. Harik [b,*], Wei-Xin Ren [c]

[a] *Parsons Brinkckerhoff, Inc., 510 First Avenue North, Suite 500, Minneapolis, MN 55403, USA*
[b] *Department of Civil Engineering, University of Kentucky, Lexington, KY 40506-0281, USA*
[c] *Department of Civil Engineering, Fuzhou University, Fuzhou, Fujian Province 350002, People's Republic of China*

Received 3 March 2001; received in revised form 18 February 2002

Abstract

A layerwise (zigzag) finite element formulation is developed for the buckling analysis of stiffened laminated plates. The laminated plate is discretized into layers along the thickness direction. Each layer of the laminated plate is modeled by the degenerated shell elements, and the stiffener is modeled by the general 3-D beam elements. Layers are stacked together according to the interlayer continuity. In-plane displacements are considered in the derivation of geometric stiffness matrix. The advantage of the proposed model is its applicability to both thin and thick laminated plates. The significance of this study lies in the disclosure of the interaction between the lateral buckling of the stiffener and the buckling of the laminate. The inverse iteration method is adopted to extract the lowest eigenvalue corresponding to buckling. Parametric and comparative studies are conducted for different plate aspect ratios, plate thickness to length ratios, degrees of layer orthotropy, ply orientations, and stiffener depth to plate thickness ratios.

Keywords: Buckling; Lateral buckling; Composite; Laminated plates; Stiffener; Finite element method; Layerwise model; Eigenvalue

1. Introduction

Eccentrically stiffened plates are widely used as components of structural systems in civil, aerospace, marine and automotive industries. Stiffeners are commonly attached to plates along the major load-carrying directions to achieve higher stiffness/weight and strength/weight ratios. To increase further, laminated composites have been first introduced in the aerospace industry, and currently being used in the civil engineering infrastructure such as bridge decks, bridge girders, strengthening and retrofitting existing structures, etc.

A comprehensive review on the literature regarding the buckling of unstiffened laminated plates was carried out by Leissa (1987). With a few exceptions, most of the existing analytical solutions are based on the classical laminate theory. Although the first-order shear deformable models are able to include the effect

* Corresponding author. Tel.: +1-859-257-3116; fax: +1-859-257-4404.
E-mail address: iharik@engr.uky.edu (I.E. Harik).

0020-7683/02/$ - see front matter
PII: S0020-7683(02)00232-9

Nomenclature

a, b	plate length in x-direction and y-direction respectively
b_s	breadth of stiffener cross-section
c_{11}	$E_1/(1-v_{12}v_{21})$, material stiffness coefficient in laminar coordinates
d	depth of stiffener cross-section
D_o	$c_{11}h^3/12$, laminate flexural rigidity in laminar coordinates
E_1, E_2	elastic moduli in fibre principle directions
G_{12}, G_{23}, G_{31}	shear moduli with respect to fiber principle directions
h	laminate thickness
h_L	thickness of a plate element in element layer L (Figs. 4 and 5)
r, s, t	natural coordinates where t is in the direction of normal
u, v, w	translational displacement in global axis x-, y- and z-direction
x, y, z	global (Cartesian) coordinates
θ	ply angle, from global x-axis to fiber direction
$\theta^x\theta^y\theta^z$	rotational displacements with respect to the global coordinates
λ	buckling stress coefficient
σ_{cr}	critical stress for initial buckling
σ_x, σ_y	initial stress in global x- and y-axes respectively
v_{ij}	Poisson's ratio, transverse strain in j-direction due to stress producing unit strain in i-direction, when stressed in the i-direction

of the transverse shear deformation, their drawbacks are addressed in the uncertainties in the calculation of the shear correction factor k. The value of $k = 5/6$ proposed by Mindlin (1951) for isotropic plate was used by Reddy (1984) to analyze laminated plates. Noor (1975) evaluated the values of k for cross-ply laminates using the 3-D elasticity theory. Different k values were obtained in the x–z plane and y–z plane for symmetric laminates, e.g. $k_{xz} = 0.8274$ and $k_{yz} = 0.5412$. The difference decreases as the number of layers increases, but significant difference exists even for laminates with a fairly large number of laminae, for instance, $k_{xz} = 0.934666$ and $k_{yz} = 0.84676$ for nine-layer symmetric laminates. For modeling thick plates, the shear correction factor k must depend on the thickness. But the derivation of a generic value of k is likely at least as involved as the development of alternative models other than the first-order shear deformable model.

The refined shear deformable models, such as higher order model, layerwise model and 3-D elasticity model, serve as alternatives to the first-order shear deformable models in the analysis of bare laminates. The higher order shear deformable model was used for the buckling of laminated plates by Reddy and Phan (1985). A static analysis of stiffened laminates was performed by Biswal and Ghosh (1994) using this model. The 3-D elasticity models are the most sophisticated but very much demanding on computer resources. This model was used by Noor (1975) for buckling of laminated plates. The generalized laminate theory based on the idea of layerwise modeling was developed by Reddy (1987). Applying this theory, Reddy et al. (1989) carried out an investigation on the stress in laminated plates, and Barbero (1989) worked on the free vibration and delamination buckling analyses of laminated plates. A geometrically exact multilayer structural theory has been developed more recently (Vu-Quoc et al., 2000).

Analysis of laminated anisotropic plates reinforced by stiffeners is complex. The numerical methods used by many researchers are the best possible approach for computation of such structures. The effort has been made to include stiffener characteristics into the plate/shell elements. The importance of the torsional ri-

gidity of the stiffener is also discussed in the literature (Venkatesh and Rao, 1985; Bhimaraddi et al., 1989). The buckling performance of stiffened composite panels was studied using finite strip method based on the classical laminate theory by Loughlan (1994).

In this paper, a layerwise finite element formulation is presented for the buckling analysis of stiffened laminated plates. In addition to the in-plane discretization (x–y plane mesh), the laminated plate is discretized into layers along the thickness direction (z-mesh). The degenerated shell elements and the general 3-D beam elements are used to represent the layers and the stiffeners, respectively. Discrete constraints are applied at nodal DOFs to accomplish the displacement continuity at the layer interface and at plate–stiffener interface. In order to achieve smooth shear distribution across thickness, bilinear constraints are applied to retain the independent transverse shear deformations in both layers adjacent to the interface instead of using the conventional linear constraints. The effects of membrane displacements are also considered in the derivation of the geometric stiffness matrix. The interaction between the lateral buckling of the stiffener and the buckling of the laminate can be included. The advantage of the proposed model is its applicability to both thin and thick laminated plates. For axially compressed laminated plates, their buckling behavior can be seriously influenced by the imperfection sensitivity (Hui, 1986). The current finite element formulation can easily account for ant kind of initial geometrically imperfections.

2. Finite element formulation

2.1. Basic assumptions

The following assumptions are made in developing the finite element formulation for the stiffened laminated plates:

- Deformations in each layer follow the Mindlin hypothesis. However, the transverse shear deformations in adjacent layers are not necessarily equal. Consequently, the variation of in-plane displacements in the thickness direction exhibits a zigzag shape.
- Transverse normal stresses are neglected. Under this assumption, the homogeneous equilibrium in the transverse direction is not satisfied in the element formulation. Therefore, the zigzag model is referred to as a 3-D model with 2-D kinematic constraints.
- Stiffeners are assumed to have rectangular cross sections and warping of cross section is not considered. The stiffeners can also be modeled as laminated plate, but these laminates are restricted to such that laminae are perpendicular to the plate.

A typical stiffened laminated plate and its coordinate definitions are shown in Fig. 1. Nine-node isoparametric shell element as shown in Fig. 2, and a 3-D isoparametric straight beam element as shown in Fig. 3 are used in the present work to model the plate/laminate and the stiffener, respectively. A layer, herein, means an entity generated by discretizing the plate along thickness direction (z-mesh), and may not necessarily represent a physical layer. It may actually represent a subdivision of a physical layer. Depending on the number of layers generated by the 3-D mesh, the resulting model can be classified as a first-order shear deformable model (one layer in the z-mesh) or a higher order shear deformable model (three or more layers in the z-mesh). In the present investigation, the number of element layers is assumed to be equal to the number of laminae.

The generalized form of the buckling eigenvalue problem using finite element discretization can be written as

$$K + \lambda K_{\mathrm{G}} = 0 \tag{1}$$

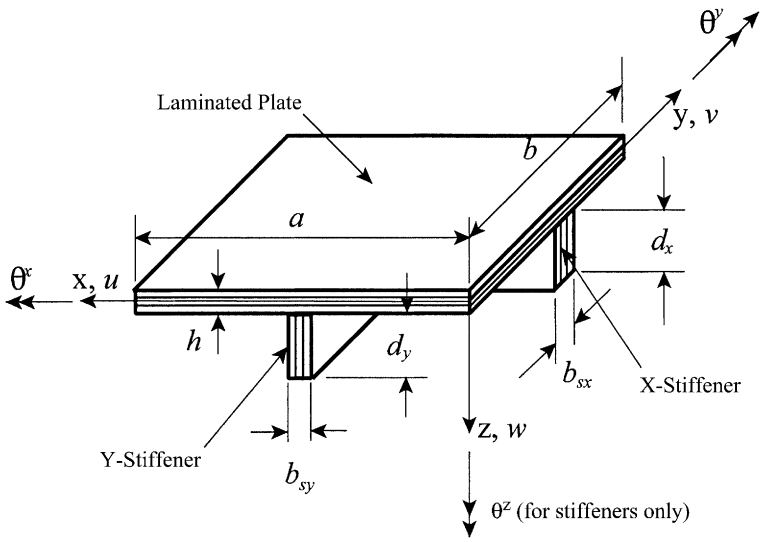

Fig. 1. Eccentrically stiffened laminated plate.

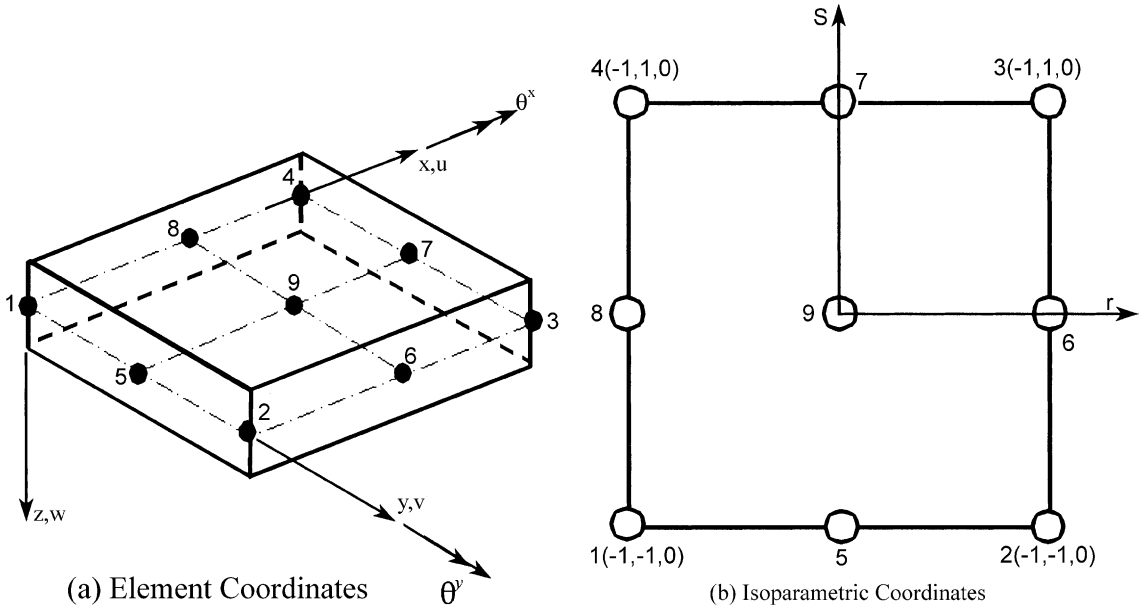

Fig. 2. 9-Noded isoparametric shell element.

where K is the elastic stiffness matrix, K_G the geometric stiffness matrix and λ represents the buckling eigenvalue. The derivation of the elastic and geometric element stiffness matrices are presented in the following sections.

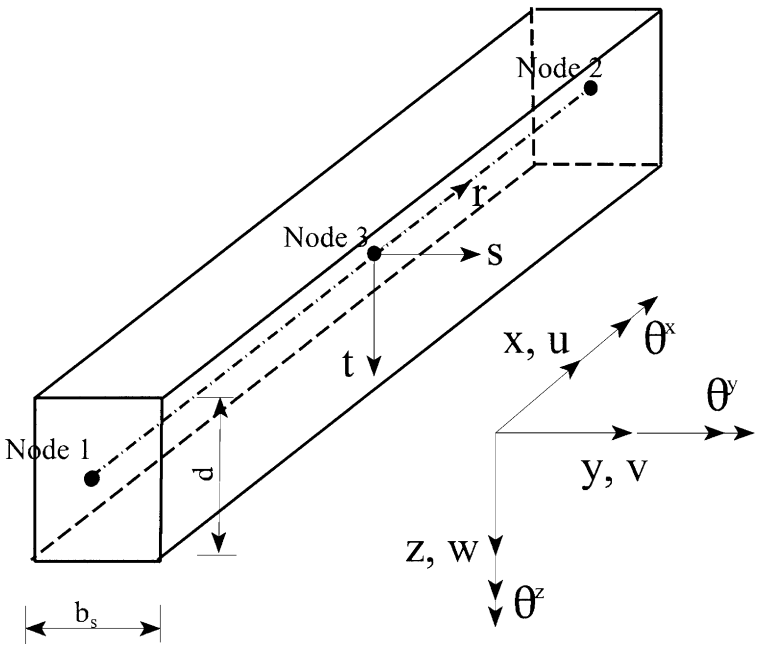

Fig. 3. 3-D isoparametric beam element.

2.2. Element stiffness matrix

As there is no substantial difference in the formulation of isoparametric shell and beam elements, the procedure adopted here for the derivation of element matrices is applicable to both the elements.

The displacements at any point in the element are interpolated as

$$\{u \quad v \quad w\}^{\mathrm{T}} = \sum_{k=1}^{n} H_k \delta_k^{\mathrm{e}} \tag{2}$$

where n is the number of nodes per element; $\{\delta_k^{\mathrm{e}}\} = \{u_k\ v_k\ w_k\ \theta_k^x\ \theta_k^y\}^{\mathrm{T}}$, $\{u_k\ v_k\ w_k\ \theta_k^x\ \theta_k^y\ \theta_k^z\}^{\mathrm{T}}$ represents the displacements at node k, for the shell and beam element respectively; and H_k is the matrix of generalized shape functions. For node k, the shape function matrix can be written as

$$[H_k] = N_k(r,s)([I][P]) \tag{3}$$

in which

$$P_{\mathrm{shell}} = t\frac{h_L}{2}\begin{bmatrix} 0 & 1 \\ -1 & 0 \\ 0 & 0 \end{bmatrix}, \qquad P_{\mathrm{beam}-x} = \begin{bmatrix} 0 & t\frac{d}{2} & -s\frac{b_s}{2} \\ -t\frac{d}{2} & 0 & 0 \\ 0 & 0 & 0 \end{bmatrix}, \qquad P_{\mathrm{beam}-y} = \begin{bmatrix} 0 & t\frac{d}{2} & 0 \\ -t\frac{d}{2} & 0 & -s\frac{b_s}{2} \\ 0 & 0 & 0 \end{bmatrix} \tag{4}$$

where $N_k(r,s)$ is the shape function in terms of Lagrangian polynomials for node k (Bathe, 1982); r, s and t are the natural coordinates (see Figs. 2 and 3); h_L is the thickness of the element layer (Fig. 4); b_s and d are the breadth and depth of the stiffener; and the matrix P represents the rotational contribution to the displacement at an arbitrary point. P_{shell}, $P_{\mathrm{beam}-x}$, and $P_{\mathrm{beam}-y}$ are the P matrices for the shell element, beam element along x-direction and beam element along y-direction, respectively. I is the identity matrix of size 3×3.

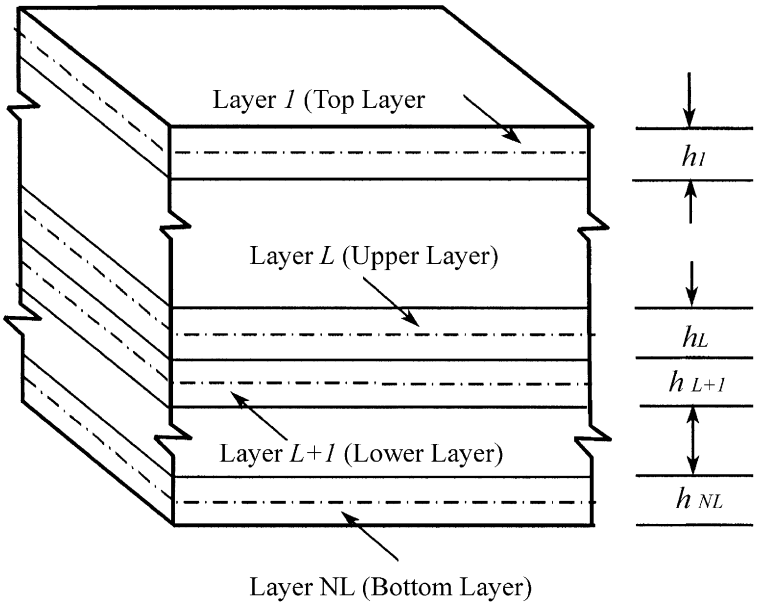

Fig. 4. Finite element mesh in thickness direction (NL = number of element layer). (—) Layer interface, where continuity is attained; (-·-·-) layer middle plane, where nodes are located.

The strain–displacement relationship that include all shear strain components except transverse normal strain is expressed as

$$\{\,\epsilon_x \quad \epsilon_y \quad \gamma_{yz} \quad \gamma_{zx} \quad \gamma_{xy}\,\}^{\mathrm{T}} = \sum_{k=1}^{n} B_k \delta_k^{\mathrm{e}} \tag{5}$$

The matrix B_k in Eq. (5) represents the strain–displacement matrix which is derived as follows:

$$B_k = [B_{k1} \quad B_{k2} \quad \cdots \quad B_{\mathrm{k5}}]^{\mathrm{T}} \tag{6a}$$

$$B_{ki} = J_{ii}^{-1} \frac{\partial H_k^{(i)}}{\partial r_i} \quad (\text{for } i = 1,2, \text{ and } r_1 = r \text{ and } r_2 = s) \tag{6b}$$

$$B_{k3} = J_{22}^{-1} \frac{\partial H_k^{(3)}}{\partial s} + J_{33}^{-1} \frac{\partial H_k^{(2)}}{\partial t} \tag{6c}$$

$$B_{k4} = J_{11}^{-1} \frac{\partial H_k^{(3)}}{\partial r} + J_{33}^{-1} \frac{\partial H_k^{(1)}}{\partial t} \tag{6d}$$

$$B_{k5} = J_{11}^{-1} \frac{\partial H_k^{(2)}}{\partial r} + J_{22}^{-1} \frac{\partial H_k^{(1)}}{\partial s} \tag{6e}$$

where $H_k^{(L)}$ is the Lth row of H_k; J_{ii}^{-1} the ith diagonal element of the matrix J^{-1}; and J the Jacobian matrix.

The Jacobian matrices for the shell element, beam element along x-direction and beam element along y-direction can be obtained respectively as

$$J_{\text{shell}} = \begin{bmatrix} \frac{a_e}{2} & 0 & 0 \\ 0 & \frac{b_e}{2} & 0 \\ 0 & 0 & \frac{h_L}{2} \end{bmatrix}, \quad J_{\text{beam}-x} = \begin{bmatrix} \frac{l_e}{2} & 0 & 0 \\ 0 & \frac{b_s}{2} & 0 \\ 0 & 0 & \frac{d}{2} \end{bmatrix}, \quad J_{\text{beam}-y} = \begin{bmatrix} \frac{b_s}{2} & 0 & 0 \\ 0 & \frac{l_e}{2} & 0 \\ 0 & 0 & \frac{d}{2} \end{bmatrix} \tag{7}$$

where a_e and b_e are the lengths of the shell element along x- and y-directions, respectively, and l_e is the length of the beam element.

Following the procedure of minimization of total potential energy, the submatrix of the element stiffness matrix, corresponding to nodes i and j, can be obtained as

$$K_{ij}^e = \frac{V_e}{8} \int \int \int B_i^T D B_j \, dr \, ds \, dt \quad (i, j = 1, 2, \ldots, n) \tag{8}$$

where D is the material stiffness matrix with respect to the global coordinates and V_e the volume of the element.

2.3. Geometric stiffness matrix

The presence of compressive stresses in laminates can result into a loss of stiffness. This loss of stiffness is accounted for by means of the geometric stiffness matrix (also known as initial stress matrix). Most of the earlier research works considered only the contribution of out-of-plane displacements in deriving the geometric stiffness matrix. The present work also takes into account the effects of in-plane displacements in addition to flexural displacements. Therefore, Green's strains are used instead of von Kármán's strains in the following derivations. The Green's strains are expressed as

$$\{\epsilon\} = \{\epsilon^l\} + \{\epsilon^{nl}\} \tag{9}$$

where $\{\epsilon^l\} = \{\epsilon_{xx} \; \epsilon_{yy} \; \gamma_{yz} \; \gamma_{zx} \; \gamma_{xy}\}^T$ is the linear strain; and $\{\epsilon^{nl}\}$ the geometric nonlinear strain whose components are

$$\epsilon_{ij}^{nl} = \frac{1}{2} \sum_{m=1}^{3} \frac{\partial u_m}{\partial x_i} \frac{\partial u_m}{\partial x_j} \quad (\text{for } i, j = 1, 2) \tag{10}$$

where $u_m = u, v,$ and w for $m = 1$, 2, and 3, respectively.

From Eq. (10), the matrix form of the nonlinear strain $\{\epsilon^{nl}\}$ is represented as

$$\epsilon^{nl} = \frac{1}{2} A \, \Omega, \tag{11}$$

where

$$\Omega = [\Omega_1 \; \Omega_2] \tag{12}$$

and

$$A = \begin{bmatrix} \frac{\partial w}{\partial x} & 0 \\ 0 & \frac{\partial w}{\partial y} \\ \frac{\partial w}{\partial y} & \frac{\partial w}{\partial x} \end{bmatrix} \tag{13}$$

The elements of the vector Ω in Eq. (12) can be written as

$$\Omega_i = \begin{bmatrix} \frac{\partial u_1}{\partial x_i} & \frac{\partial u_2}{\partial x_i} & \frac{\partial u_3}{\partial x_i} \end{bmatrix}^T \quad (\text{for } i = 1, 2) \tag{14}$$

Again, with the displacement interpolation described in Eq. (1), Eq. (14) can be expressed as

$$\Omega = \sum_{k=1}^{n} G_k \delta_k^{\mathrm{e}} \tag{15}$$

in which G_k is a 6×5 matrix for the shell element and a (6×6) matrix for the beam element. The rows in G_k are defined by

$$G_{ki} = J_{11}^{-1} \frac{\partial H_k^{(i)}}{\partial r} \quad (\text{for } i = 1, 2, 3) \tag{16a}$$

$$G_{ki} = J_{22}^{-1} \frac{\partial H_k^{(i-3)}}{\partial s} \quad (\text{for } i = 4, 5, 6) \tag{16b}$$

Each sub-block of the element geometric stiffness matrix (Zienkiewicz, 1977), representing the contribution of node j to i can be obtained as

$$K_{G_{ij}}^{\mathrm{e}} = \frac{V_{\mathrm{e}}}{8} \int\int\int G_i^{\mathrm{T}} \sigma^0 G_j \, \mathrm{d}r \, \mathrm{d}s \, \mathrm{d}t \quad (\text{for } i, j = 1, 2, \ldots, n) \tag{17}$$

where σ^0 is the initial stress matrix with respect to the global coordinates. The initial stress matrix can be expressed as

$$\sigma^0 = \begin{bmatrix} \sigma_x I & \tau_{xy} I \\ \text{sym} & \sigma_y I \end{bmatrix} \tag{18}$$

where I is the identity matrix of size 4×4.

2.4. Interlayer continuity

Since there are no nodes in the surface of the shell or the beam element, no common nodes are shared by the elements in adjacent layers as shown in Fig. 5. Since the displacements in a stack are all coupled after the interface constraints are applied, the column heights determining the skyline of the global stiffness matrix are calculated in terms of element stacks instead of individual elements. In order to attain the displacement continuity in the element layer interfaces (interlayer continuity), constraints are explicitly imposed to the nodal DOFs. The continuity of the in-plane displacement v between layer L and $L+1$ is illustrated in Fig. 5(a). The constraint equation for v is established by means of the displacements at the reference points $P_{L+1/2}$, which is the projection of node points P_L and P_{L+1} at the interface and has a new location $P'_{L+1/2}$ after deformation. Based on the interlayer continuity, the in-plane displacement $v_{L+1/2}$ at the reference point, determined by the displacement v_L and θ_L^x of layer L, or v_{L+1}^x of layer $L+1$, must be identical. The same rule applies to $u_{L+1/2}$. Thus, the interlayer constraining relationship for the in-plane displacements u, v can be derived as follows:

$$u_L + \frac{h_L}{2}\theta_L^y = u_{L+1} - \frac{h_{L+1}}{2}\theta_{L+1}^y \quad (\text{for } L = 1, 2, \ldots, \mathrm{NL} - 1) \tag{19a}$$

$$v_L - \frac{h_L}{2}\theta_L^x = v_{L+1} + \frac{h_{L+1}}{2}\theta_{L+1}^x \quad (\text{for } L = 1, 2, \ldots, \mathrm{NL} - 1) \tag{19b}$$

With the intention of eliminating the rotations in the $(L+1)$ layer, Eqs. (19a) and (19b) are rearranged into:

$$\theta_{L+1}^y = (u_{L+1} - u_L)\frac{2}{h_{L+1}} - \theta_L^y \frac{h_L}{h_{L+1}} \quad (\text{for } L = 1, 2, \ldots, \mathrm{NL} - 1) \tag{20a}$$

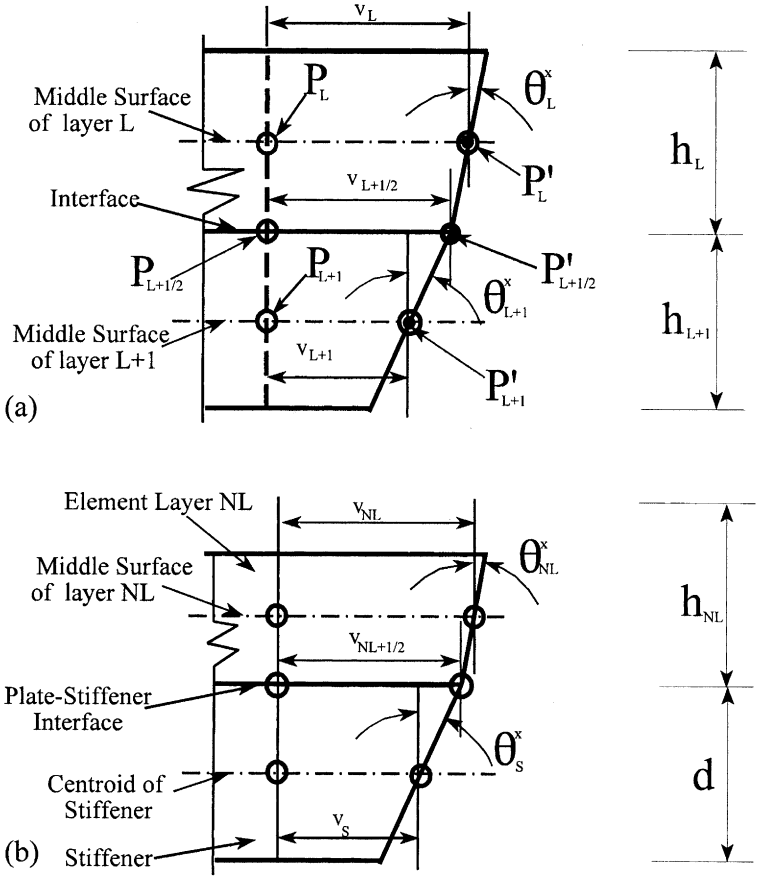

Fig. 5. Bilinear (a) interlayer continuity and (b) plate–stiffener continuity.

$$\theta^x_{L+1} = -(v_{L+1} - v_L)\frac{2}{h_{L+1}} - \theta^x_L \frac{h_L}{h_{L+1}} \quad (\text{for } L = 1, 2, \ldots, \mathrm{NL} - 1) \tag{20b}$$

It is evident from Fig. 5 that this constraint cannot be accomplished by using rigid arms because a rigid arm remains straight and does not allow the slope change at the reference point. Physically, the constraint Eqs. (19a) and (19b) or (20a) and (20b) represent two rigid arms connected at the reference point by a universal ball joint. Because of this, they are known as bilinear constraints in order to be distinguished from the constraints imposed by adding rigid arms.

Eqs. (19a), (19b), (20a), (20b) are in connection with two elements in two adjacent element layers. Thus, the constraints cannot be introduced to the equilibrium equations at element level. It must be implemented when the global stiffness matrix is being setup. Meanwhile, θ^x_{L+1} and θ^y_{L+1} are eliminated except in the top layer. Since the remaining degrees of freedom are predictable after the nodes and boundary conditions are defined, the degrees of freedom to be eliminated are not numbered. Therefore, there is no additional change in the skyline of the global matrices due to the elimination.

The constraint equations are also valid for the inter-element connection at the stiffener–plate interface. In this case, L equals NL where the layer $L + 1$ (=NL + 1) denotes the beam layer, while h_{L+1} is replaced by the depth of stiffener d. At the node where different stiffeners intersect, the stiffener depths in the x- and the y-directions are given the corresponding stiffener depths d_x and d_y as shown in Fig. 5(b).

3. Numerical results and discussions

The correctness of the finite element model proposed for the buckling analysis of stiffened laminated plates in the previous sections is verified by comparing the numerical results with the available analytical solutions. The inverse iteration method is adopted to extract the lowest eigenvalue corresponding to buckling. A 4×8 finite element mesh is used for the in-plane layers of the plate. A uniformly reduced (2×2) integration scheme is adopted for both shell and beam elements. In the following sections, results are presented for unstiffened anisotropic plates, stiffened isotropic plates, stiffened orthotropic and stiffened laminated plates.

3.1. Unstiffened anisotropic plates

The significance of orthotropic ratio E_1/E_2 and thickness to length ratio h/a in the buckling behavior is investigated separately. A parametric study is conducted using the proposed finite element model for the buckling analysis of thick plates and laminates. The variation of buckling coefficients against the ratio of depth of stiffener to thickness of laminate, d/h, is investigated. The results obtained are compared with the 3-D elasticity solution given by Noor (1975).

A two and three layered cross-ply square plate with the lay-up of $0°/90°$ (NL = 2) and $0°/90°/0°$ (NL = 3), as shown in Fig. 6, are analyzed under uniaxial compression along x-direction. All the sides of the plate are simply supported. The material properties are $G_{12}/E_2 = G_{31}/E_2 = 0.6$, $G_{23}/E_2 = 0.5$ and $v_{12} = 0.25$. From the analysis, buckling coefficients for various ratio of orthotropy E_1/E_2 are obtained for a laminate thickness to length ratio $h/a = 0.1$. The results are presented in Fig. 6, and they comparable with the 3-D elasticity solution presented by Noor (1975).

The buckling coefficients for plate thickness to length ratios h/a ranging from 0.01 to 0.20 are studied for a degree of orthotropy $E_1/E_2 = 30$ and the results are shown in Fig. 7. The ratio of buckling coefficients $\Lambda = \lambda/\lambda°$ is plotted against the thickness to length ratio h/a. The buckling coefficient $\lambda = \sigma_{cr}a^2/(E_2h^2)$ is the one determined from the proposed finite element model and $\lambda° = \sigma_{cro}a^2/(E_2h^2)$ depends on the critical stress σ_{cro} which is based on the classical laminate theory (Jones, 1975). In this study, the solution by classical laminate theory is used only for the calculation of buckling coefficient $\lambda°$ of symmetric cross-ply plates. Similar solution for skew-symmetric laminates is available to calculate the critical stresses based on the classical laminate theory. However, in the present work, it is not used in determining the buckling coefficients of the skew-symmetric laminate in Fig. 7. Instead, the buckling coefficient computed from the present finite element method for a plate thickness to length ratio $h/a = 0.01$ is used. In fact, at this thickness ratio, the buckling coefficient of the symmetric laminate determined from the present analysis deviates from the classical laminate theory solution only by 0.07%. The results shown in Fig. 7 agree well with the 3-D elasticity solution reported by Noor (1975).

3.2. Stiffened single layer plates

Having verified the convergence of the present finite element model for simple plates in the previous section, it is further used to analyze stiffened plates in which the stiffeners are modeled as beam elements. There are two cases analyzed under this category: one is a stiffened isotropic plate and another is a stiffened orthotropic plate. These two problems are solved mainly to verify the performance of proposed shell and eccentric beam elements in modeling the stiffened plates under in-plane compression.

3.2.1. Stiffened isotropic single layer plate

A stiffened rectangular isotropic plate as shown in Fig. 8 is studied for buckling behavior under uniaxial in-plane compression along x-direction. The stiffener is located at the center of the panel along the direction

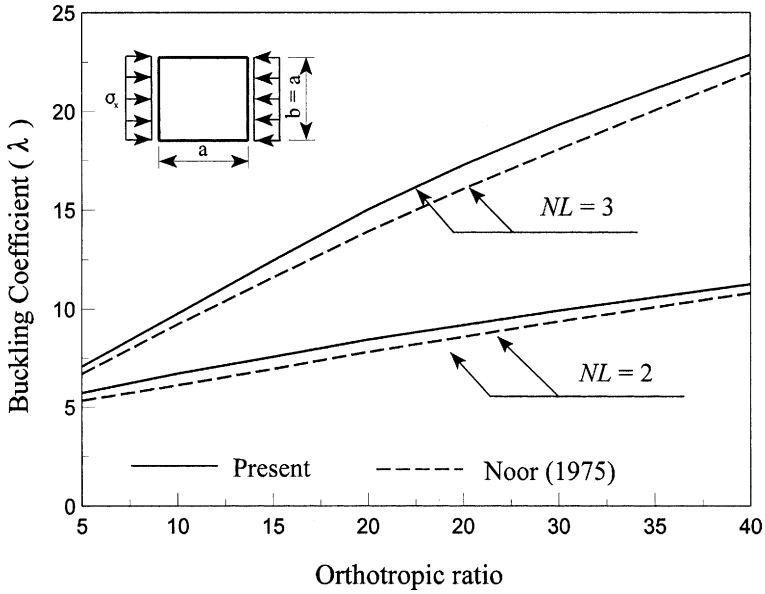

Fig. 6. Buckling coefficients of a simply supported cross-ply square laminate with orthotropic ratio (NL = number of layers).

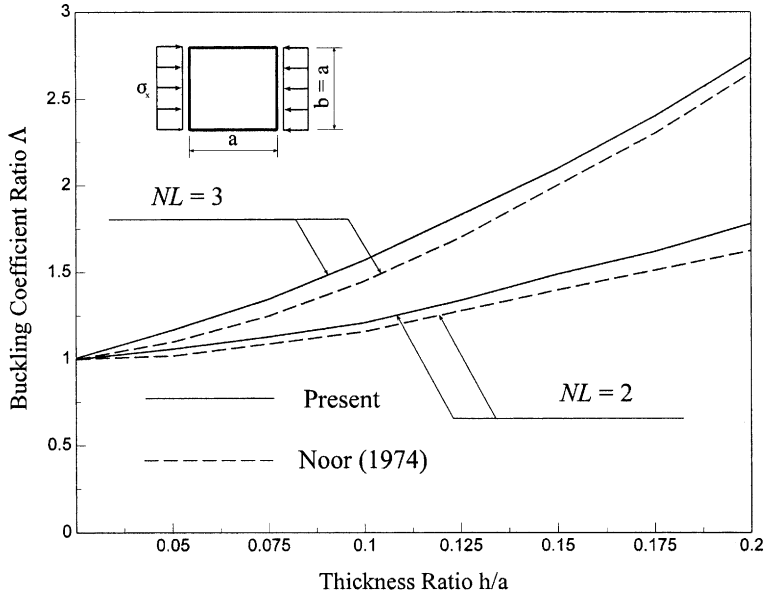

Fig. 7. Buckling coefficients ratio of a simply supported cross-ply square laminate with thickness to length ratio (NL = number of layers).

of compression. Both the plate and the stiffener are simply supported on all sides and the material properties are assumed to be isotropic with Poisson's ratio $v = 0.3$. The plate thickness to length ratio is taken as 0.01, and this corresponds to a thin plate situation. The buckling coefficient $\lambda = \sigma_{cr} b^2 h/(\pi^2 D_o)$ is computed

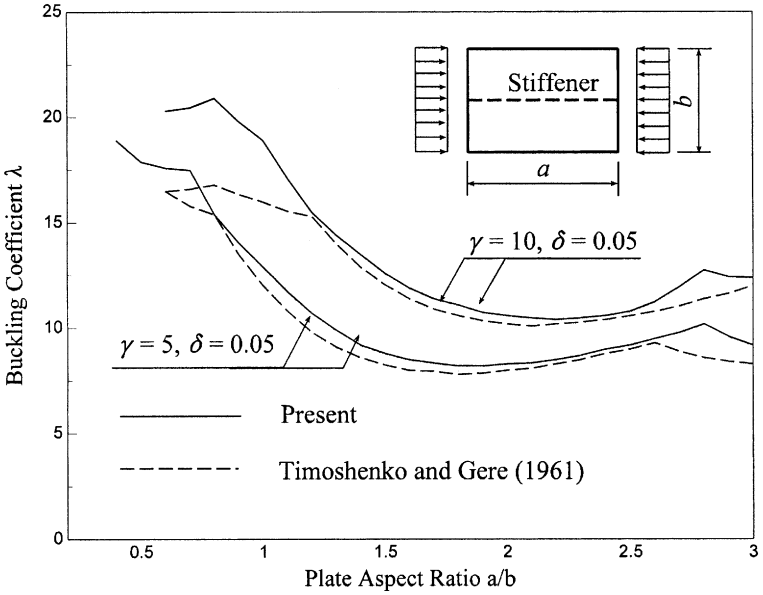

Fig. 8. Buckling coefficient of a stiffened isotropic plate with plate aspect ratio ($I_s = b_s d^3/3$, $\gamma = I_s/bD_o$, $h/a = 0.01$ and $\delta = b_s d/bh$).

for plate aspect ratios a/b ranging from 0.6 to 3.0. σ_{cr} is the critical stress; b the width of the plate, and the flexural rigidity $D_o = Eh^3/12(1-\nu^2)$.

In the case of $h/a = 0.01$, as shown in Fig. 8, the results of the present finite element model are not expected to be significantly different from the ones obtained from the thin plate theory (Timoshenko and Gere, 1961). However, for the smaller aspect ratios ($0.6 < a/b < 1.0$), the difference increases with the size of the stiffener (larger $\gamma = I_s/bD_s$). This difference is attributed to the neglect of the torsional rigidity of the stiffener in Timoshenko and Gere's derivation (1961). When the plate is short in the stiffener direction (smaller a/b), the plate tends to buckle in a mode that is antisymmetric about the stiffener. As a result, the stiffener is twisted and the torsional rigidity of the stiffener becomes very effective. This leads to higher buckling coefficients. The torsional rigidity of the stiffener does not affect the buckling load if the stiffener is not twisted as the plate buckles for large a/b. For larger a/b values, the difference in the buckling coefficients in Fig. 8 can be due to the assumption that in-plane displacements are negligible, and due to the fact that the moment of inertia of the stiffener (I_s) is computed with respect to the plate–stiffener interface in Timoshenko and Gere's derivations.

3.2.2. Stiffened orthotropic single layer plates

A stiffened orthotropic rectangular plate, as shown in Fig. 9, is studied under uniaxial compression along y-direction. The single layer plate is centrally stiffened along the y-direction. Parametric studies were conducted for plate aspect ratios a/b and stiffener depth to plate thickness ratios d/h. The width of the stiffener is assumed to be equal to the plate thickness h for all cases. The plate thickness to length ratio is kept as $h/a = 0.01$. The strong material direction coincides with the x-axis of the plate and the longitudinal direction of the stiffener. The material is assumed to be E-glass/Epoxy possessing the following properties: $E_1 = 60.7$ GPa (8.8×10^3 ksi), $E_2 = 24.8$ GPa (3.6×10^3 ksi), $G_{12} = G_{31} = G_{23} = 12.0$ GPa (1.7×10^3 ksi) and $\nu_{12} = 0.23$. The buckling coefficient is defined as $\lambda = \sigma_{cr} a^2 h/D_o$, where the flexural rigidity $D_o = E_1 h^3/12(1-\nu^2)$.

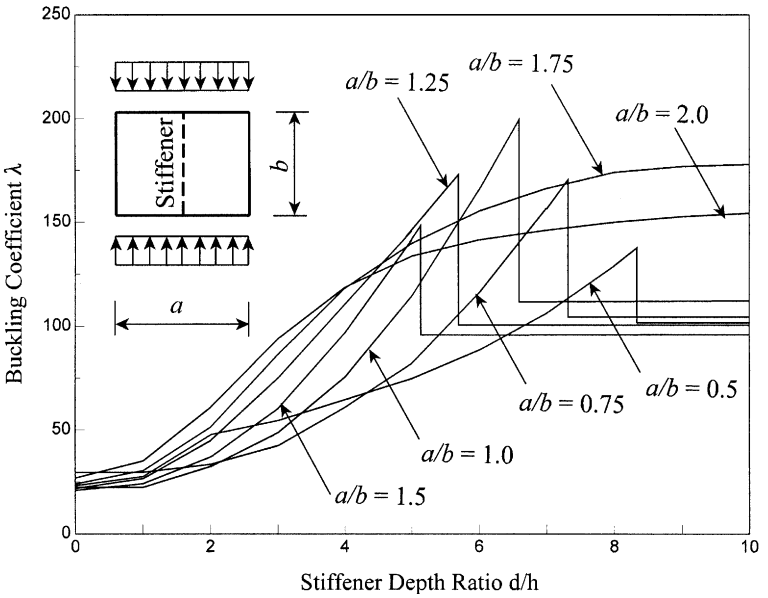

Fig. 9. Buckling coefficient of a stiffened orthotropic plate with stiffener depth to plate thickness ratio.

The buckling coefficients and mode shape transition are given in Figs. 9 and 10 for stiffener depth to plate thickness ratios d/h varying from 0.01 to 10, and plate aspect ratios a/b varying from 0.5 to 2.0. It is demonstrated that for square plates ($a/b = 1.0$), as d/h reaches 6.665, the buckling coefficient λ drops suddenly (snapping) from $\lambda = 204$ to $\lambda = 104$ and then remains constant for $d/h > 6.665$. The buckling mode shifts from a saddle shape into a double antisymmetric shape as shown in Fig. 10. This does not occur with rectangular plates with large aspect ratios ($a/b > 1.75$). The results revealed from parametric studies (Guo, 1996) show that the lateral stability of the stiffener has a significant impetus on the buckling of the plate. For plates with stiffeners having a small depth, the buckling is initiated by plate itself. If the stiffener is very deep, the buckling of a stiffened plate may be initiated by lateral buckling of the stiffener. The stability of the stiffener is also affected by the torsional restraint provided by the plate flexural rigidity.

3.3. Stiffened laminated plates

3.3.1. Stiffened symmetric cross-ply laminated plates

A simply supported square stiffened laminated plate with symmetric cross-ply (90°/0°/90°) configuration is analyzed under uniaxial compression along the x-direction as shown in Fig. 11. The laminated plate is stiffened at the center along the direction of compression. The material properties of the stiffener and laminate are $G_{12}/E_2 = G_{31}/E_2 = 0.6$, $G_{23}/E_2 = 0.5$ and $v_{12} = 0.25$. The stiffener is assumed to be along the strong axis.

Parametric studies are conducted for various degrees of orthotropy $R = E_1/E_2$ and for different stiffener depth to laminate thickness ratios d/h. The thickness to length ratio h/a is kept as 0.05, and the stiffener width b_s is assumed to be equal to the laminate thickness. The buckling coefficients $\lambda = \sigma_{cr}a^2/(E_2h^2)$ obtained from the present study are given in Fig. 11. It is seen that the buckling coefficient snaps as the stiffener depth increases. This snapping is mainly due to the lateral instability of the deep stiffener. As the degree of orthotropy increases, the buckling coefficient also increases. But the ratio of stiffener depth to plate thickness at snapping (transition of mode shape) decreases with increasing degree of orthotropy. After

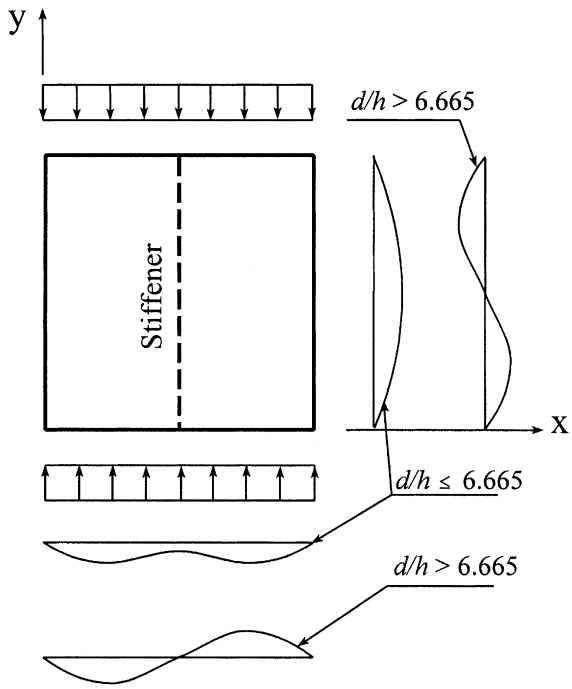

Fig. 10. Mode transition of a stiffened orthotropic square plate with stiffener depth ratio.

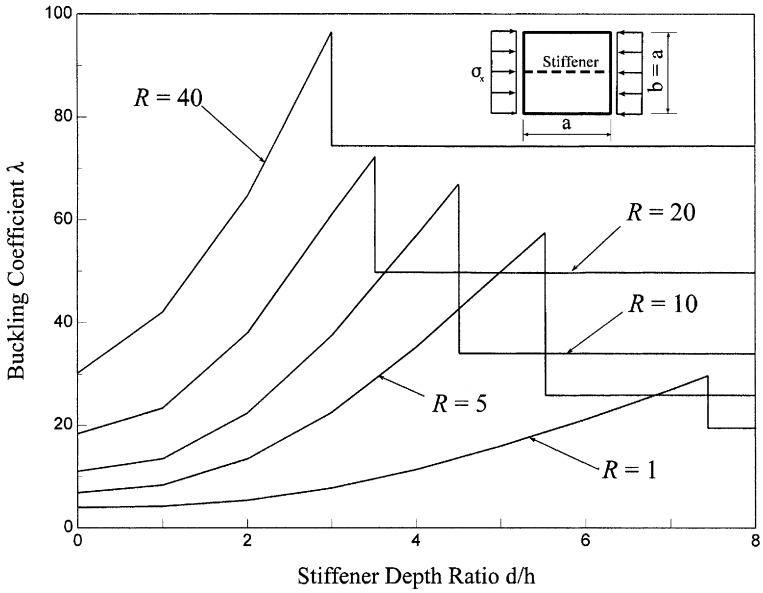

Fig. 11. Buckling coefficients of a stiffened cross-ply square laminate with stiffener depth to laminate thickness ratio.

snapping at each degree of orthotropy, the buckling coefficient remains constant for all values of stiffener depth to plate thickness ratios d/h. This shows that the stiffeners are efficient in increasing the buckling load only up to a certain value of stiffener depth.

3.3.2. Stiffened symmetric angle-ply laminated plate

A simply supported square stiffened angle-ply $(\theta/-\theta/\theta)$ laminated plate is studied under uniaxial compression along the x-direction. The laminated plate is centrally stiffened along the x-direction, and the material strong direction coincides with longitudinal axis of the stiffener. The orthotropic material properties of each layer are $G_{12}/E_2 = G_{31}/E_2 = 0.6$, $G_{23}/E_2 = 0.5$ and $\nu_{12} = 0.25$. The laminate thickness to length ratio, h/a, is taken as 0.05 and the stiffener width, b_s, is assumed to be equal to laminate thickness. The buckling coefficients $\lambda = \sigma_{cr}a^2/(E_2h^2)$ are given in Fig. 12 for ply angles θ ranging from 0° to 90°, while the change in buckling coefficients is given in Fig. 13 for stiffener depth to laminate thickness ratios d/h ranging from 0.01 to 8.

Fig. 12 shows that the variation of the buckling load with the ply angle θ for a stiffened laminate $(d/h > 0)$ which is not symmetric about $\theta = \pi/4$, as is the case for unstiffened laminates $(d/h = 0)$. Therefore, attempts to optimize either the ply angle or the stiffener depth to laminate thickness ratio must consider the full range of the ply angle $0° \leqslant \theta \leqslant 90°$. It is also noted that for $\theta < \pi/6$, the buckling coefficient λ at $d/h = 8$ is lower than the case when $d/h = 4$. This is due to the fact that the stiffener buckles laterally when $d/h = 8$, while the stiffener remains stable when $d/h = 4$.

Fig. 13 shows that the snapping in buckling coefficient does not occur in laminates with ply angle θ greater than $\pi/4$. For $\theta \leqslant \pi/3$, the buckling coefficient remains constant after stiffener depth ratio d/h reaches a value of 6, which indicates that the stiffener is acting more like an intermediate support. For the laminates with a small ply angle $(\theta < \pi/4)$, snapping in the buckling coefficients is found because of the lateral buckling of the stiffener. It is observed that the flexural stiffness of laminate provides a torsional restraint to the stiffener as the stiffener tends to buckle laterally. Recalling that the ply angle is defined as the

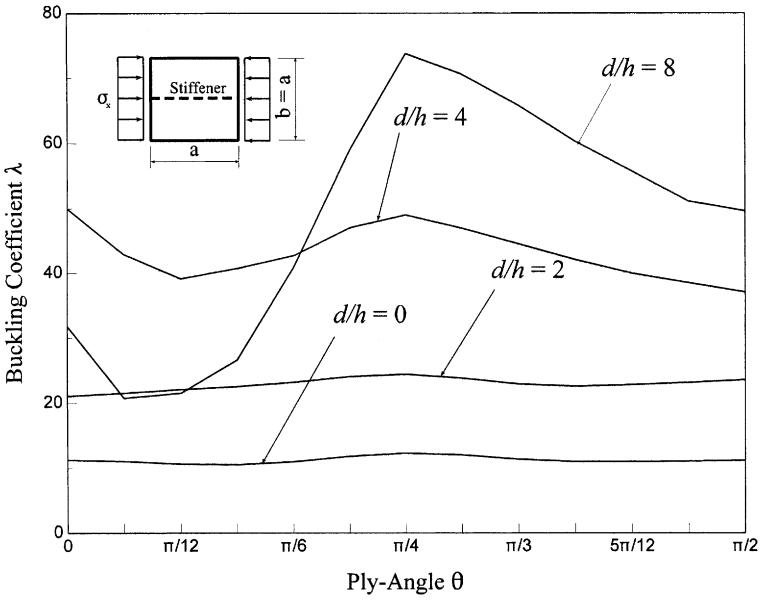

Fig. 12. Buckling coefficients of a stiffened angle-ply square laminate with ply angle.

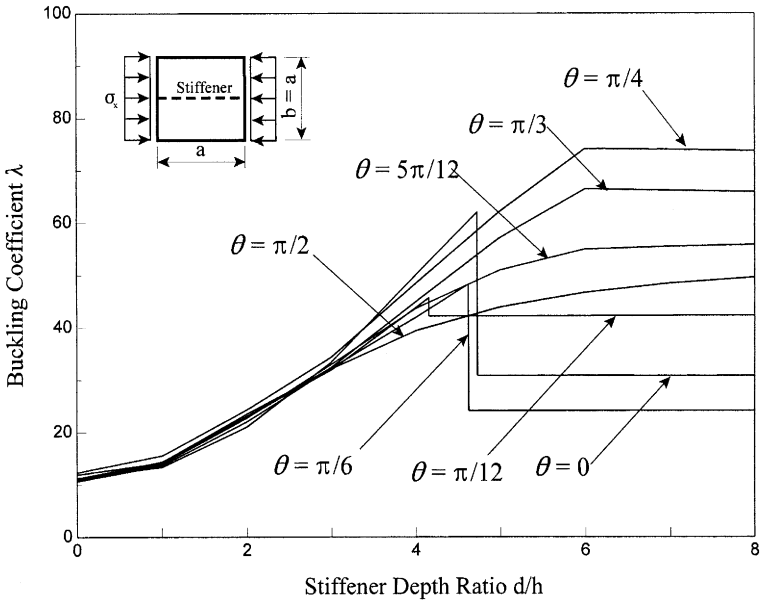

Fig. 13. Buckling coefficients of a stiffened square angle-ply laminate with stiffener depth to laminate thickness ratio.

angle from the laminate plate x-axis to the fiber direction, a laminate plate with small ply angle possesses a small flexural rigidity D_y, which leads to a smaller torsional restraint to the stiffener.

4. Conclusions

A layered (zigzag) finite element formulation is developed for the buckling analysis of stiffened plates and laminates. The procedure adopted for the derivation of the elastic and geometric stiffness matrices of the shell and beam element is presented, and the method for attaining interlayer continuity is discussed. Numerical results are presented for the buckling behavior of unstiffened and stiffened plates/laminates under uniaxial compression. The results are comparable with available solutions. A parametric study is performed with various plate aspect ratios, stiffener depth to plate thickness ratios, ply angle orientations, degrees of orthotropy and number of layers. The influence of all these parameters on the buckling load is presented and discussed.

The proposed finite element formulation can accurately predict the buckling behavior of plates/laminates for various thickness to length h/a ratios. It is demonstrated that the interactive buckling or the mode shape transition between laminated plate and stiffener plays an important role in maintaining the bucking behavior of stiffened laminated plates. A deeper stiffener leads to a higher buckling load only to a certain extent. Beyond a certain depth, the lateral instability of the stiffener can occur instead of the buckling of the laminated plate. The lateral buckling of the stiffener may result in the sudden drop of the buckling load of stiffened laminated plates. Therefore, the lateral buckling of a deep stiffener must be monitored as a critical factor to the buckling behavior of stiffened laminated plates. Since the present beam model for the stiffener includes lateral, flexural and torsional degrees of freedom, this permits the capture of the true buckling behavior of the stiffener. The interaction of stiffener lateral buckling with the buckling of laminated plates can not be revealed if a 2-D beam element is used to present the stiffener where the lateral bending stiffness is ignored.

It is found that the lateral-flexural stiffness and torsional stiffness of the stiffener are the major factors in keeping the stiffener laterally stable. The lateral buckling of the stiffener is influenced by the torsional restraining effect provided by the laminated plate. This restraining effect is determined by the flexural stiffness of the laminated plates about the stiffener that is in turn determined by the degree of orthotropy, the fiber orientation, the aspect ratio, and so forth. The convergence on element mesh becomes stringent when a relatively deep stiffener is used. Experience has shown that a mesh of 6×6 for whole laminated plate is fine enough if the stiffener is week or moderately strong. However, a finer mesh is needed if a very strong stiffener is used or the conditions follow a mode shape in the adjacent point of mode shape transition.

The numerical results have shown how the proposed finite element formulation can be used to optimize the design of compressed stiffened plates/laminates by varying the stiffener depth to plate/laminate thickness ratio d/h and/or by varying the ply angle θ. Optimization must consider the full range of the ply angle $0^\circ \leqslant \theta \leqslant 90^\circ$. It is anticipated that the finite element formulation can be used for the evaluation of the buckling behavior of the modern bridge structure made of stiffened laminated composites.

References

Barbero, E.J., 1989. On a generalized laminate theory with application to bending, vibration and delamination buckling in composite laminates. Ph.D. Dissertation. Virginia Polytechnic Institute and State University.

Bathe, K.J., 1982. Finite Element Procedures in Engineering Analysis. Prentice-Hall, Englewood Cliffs, NJ.

Bhimaraddi, A., Carr, A.J., Moss, P.J., 1989. Finite element analysis of laminated shells of revolution with laminated stiffeners. Comput. Struct. 33 (1), 295–305.

Biswal, K.C., Ghosh, A.K., 1994. Finite element analysis for stiffened laminated plates using higher order shear deformation theory. Comput. Struct. 53 (1), 161–172.

Guo, M.W., 1996. Bending, free vibration, and buckling of stiffened plates and laminates. Ph.D. Dissertation. University of Kentucky.

Hui, D., 1986. Imperfection sensitivity of axially compressed laminated plates due to bending–stretching coupling. Int. J. Solids Struct. 22 (1), 13–22.

Jones, R.M., 1975. Mechanics of Composite Materials. McGraw-Hill Company, New York.

Leissa, A.W., 1987. A review of laminated composite plate buckling. Appl. Mech. Rev. 40 (5), 575–591.

Loughlan, J., 1994. The buckling performance of composite stiffened panel structures subjected to combined in-plane compression and shear loading. Compos. Struct. 29, 197–212.

Mindlin, R.D., 1951. Influence of rotary inertia and shear on flexural motions of isotropic elastic plates. J. Appl. Mech. 73, 31–38.

Noor, A.K., 1975. Stability of multilayered composite plates. Fiber Sci. Technol. 8, 81–89.

Reddy, J.N., 1984. Energy and Variational Methods in Applied Mechanics. John Wiley & Sons Inc., New York.

Reddy, J.N., 1987. A generalization of two-dimensional theories of laminated plates. Commun. Appl. Numer. Meth. 3, 113–130.

Reddy, J.N., Barbero, E.J., Teply, J.L., 1989. A plate bending element based on a generalized laminated plate theory. Int. J. Numer. Meth. Eng. 28, 2275–2292.

Reddy, J.N., Phan, N.S., 1985. Stability and natural vibration of isotropic, orthotropic and laminated plates according to a higher order shear deformable theory. J. Sound Vib. 98 (2), 157–170.

Timoshenko, S.P., Gere, J.M., 1961. Theory of Elastic Stability, Second ed. McGraw-Hill Book Company, New York.

Venkatesh, A., Rao, K.P., 1985. Analysis of laminated shells of revolution with laminated stiffeners using a doubly curved quadrilateral finite elements. Comput. Struct. 20 (4), 669–682.

Vu-Quoc, L., Deng, H., Tan, X.G., 2000. Geometrically-exact sandwich shells: the static case. Comput. Meth. Appl. Mech. Eng. 189, 167–203.

Zienkiewicz, O.C., 1977. The Finite Element Method, third ed. McGraw-Hill, Maidenhead, Berkshire, England.